ELSEVIER

J. Non-Newtonian Fluid Mech. 144 (2007) 140–148

Journal of Non-Newtonian Fluid Mechanics

www.elsevier.com/locate/jnnfm

Divergent flow in contractions

Manuel A. Alves [a,*], Robert J. Poole [b]

[a] *Departamento de Engenharia Química, CEFT, Faculdade de Engenharia, Universidade do Porto, Rua Dr. Roberto Frias, 4200-465 Porto, Portugal*
[b] *Department of Engineering, University of Liverpool, Brownlow Street, Liverpool L69 3GH, United Kingdom*

Received 15 August 2006; received in revised form 26 February 2007; accepted 2 April 2007

Abstract

This study reports the results of a systematic numerical investigation, using the upper-convected Maxwell (UCM) model, of viscoelastic flow through 'smooth' planar contractions of various contraction ratios with particular emphasis placed on the 'divergent flow' regime. It is shown that both inertia and/or shear-thinning are not required for divergent flow to be predicted in contrast to the existing results in the literature where inertia has always been present when the phenomenon has been observed. Guided by the numerical results a simple explanation is presented for the occurrence of divergent flow and the conditions under which it arises. In addition, above a critical Deborah number, the flow becomes unsteady and we use an analysis based on the scaling laws of McKinley et al. [G.H. McKinley, P. Pakdel, A. Oztekin, Rheological and geometric scaling of purely elastic flow instabilities, J. Non-Newtonian Fluid Mech. 67 (1996) 19–47] for purely elastic instabilities to show that the square of this critical Deborah number varies linearly with contraction ratio in excellent agreement with the numerical results obtained in this study.

Keywords: Divergent flow; Viscoelastic flow in contractions; UCM model; Creeping flow; Purely elastic instability; Finite-volume method

1. Introduction

Of the many thought-provoking and striking phenomena that are observed when a viscoelastic liquid flows through a contraction geometry, perhaps the least studied is that of the "divergent flow" regime. This regime, first shown in the papers of Cable and Boger [2–4], is characterised by a strong curvature of the streamlines away from the centreline towards the duct walls some distance upstream of the contraction: almost as if some "invisible obstacle" has been placed in the liquid's path. As a consequence, the divergent flow regime results in an undershoot of the centreline velocity and is usually associated with off-centre velocity maxima. The effect is nicely illustrated in the flow visualisation book of Boger and Walters ([5] c.f. page 51), using a picture taken from the thesis of Cable [6] of flow in a 4:1 axisymmetric contraction, where the following explanation is given:

> "The conflict between inertia which tends to decrease the size of the vortex and elasticity which encourages vortex growth results in a symmetrical divergence of the streamlines".

The experiments reported in Cable and Boger were conducted before the work reported in Boger's seminal paper [7] where he first described the constant-viscosity elastic liquid which now bears his name and can be obtained by adding small amounts of high molecular weight polymer to a solvent with high viscosity. As a consequence of the difficulties in interpreting the results of Cable and Boger unambiguously, which are for shear-thinning solutions, Boger and Binnington [8] revisited the 4:1 axisymmetric contraction using the 'M1' Boger fluid. Here again divergent flow was observed at high flowrates showing that shear thinning is not necessary for the phenomenon to be observed. In the divergent flow regime the importance of inertia, although not negligible, was much less than in the earlier shear-thinning results of Cable and Boger ($Re = 0.89$ compared to order 100 in the earlier work). Despite this reduction in importance, Boger and Binnington [8] still attributed the appearance of divergent flow to inertia "winning" the interplay with elasticity.

Evans and Walters [9,10] performed a rather extensive set of visualisations for both Boger fluids and shear-thinning polyacrylamide solutions in planar contraction flows. They investigated the effect of both contraction ratio and rounding of the re-entrant corner and observed divergent flow behaviour only for relatively low concentrations of polyacrylamide where both shear-thinning and inertia played a significant role (c.f. Fig. 6 in [9]).

* Corresponding author. Fax: +351 225081449.
E-mail addresses: mmalves@fe.up.pt (M.A. Alves), robpoole@liv.ac.uk (R.J. Poole).

0377-0257/$ – see front matter © 2007 Elsevier B.V. All rights reserved.
doi:10.1016/j.jnnfm.2007.04.003

More recently Rodd et al. [11] investigated the flow of dilute aqueous polyethylene oxide (PEO) solutions through microfabricated planar (3D) abrupt contraction/expansions. Although the solutions used in the experiments were dilute, with relaxation times of the order of milliseconds, the small length scales and the high strain rates in the entrance region lead to significant extensional effects and at high Deborah numbers strongly divergent flow was observed. Again inertia was not negligible, and the authors stated that diverging flow is a hallmark of fluid elasticity, and that inertia and deformation rate-dependent material functions tend to enhance its intensity.

On the numerical side, Hulsen [12] used the shear-thinning Phan–Thien–Tanner (PTT) model [13] to investigate divergent flow in an abrupt axisymmetric contraction (i.e. identical to the geometry of [4] and [8]). In this case divergent flow was observed only when both inertial and elastic stresses were present (i.e. in general agreement with the experimental findings above). Hulsen also found that the occurrence, or otherwise, of divergent flow was sensitive to the extensional properties of the PTT model parameters and that, in particular, vortex enhancement had to be present for the effect to be seen.

Purnode and Crochet [14] used the FENE-P model [15] to simulate the flow through planar contractions, using the visualisations of Evans and Walters as a basis for comparison. The simulations were able to qualitatively capture most of the experimentally observed features including the divergent flow of a comparable concentration of PAA compared to Evans and Walters (0.25% c.f. 0.2%). Once again inertia was necessary for the divergent flow regime to be seen: when Purnode and Crochet kept the Weissenberg number fixed and neglected inertia (i.e. set $Re = 0$) a salient corner vortex enhancement mechanism was observed and the divergent region apparently disappeared.

In this study we investigate the divergent flow regime in detail and report the results of a systematic numerical investigation, using the upper-convected Maxwell (UCM) model, of viscoelastic flow through 'smooth' planar contractions of various contraction ratios. We show that both inertia and/or shear-thinning are *not* required for divergent flow to be observed. Guided by our numerical results we derive a simple explanation for the occurrence of inertialess divergent flow and the conditions under which it arises. In addition, above a critical Deborah number, the flow becomes unsteady and we use the scaling laws of McKinley et al. [1] for purely elastic instabilities to show that the square of this critical Deborah number (i.e. De^2_{crit}) varies linearly with contraction ratio in agreement with our numerical results.

2. Governing equations and numerical method

In this work we are concerned with the creeping (i.e. $Re \to 0$), isothermal flow of an incompressible viscoelastic fluid through a smooth two-dimensional contraction. The equations to solve are those of conservation of mass

$$\nabla \cdot \boldsymbol{u} = 0 \tag{1}$$

and of momentum

$$-\nabla p + \nabla \cdot \boldsymbol{\tau} = \boldsymbol{0} \tag{2}$$

and a suitable choice for the viscoelastic stress tensor $\boldsymbol{\tau}$. For reasons of rheological simplicity the well known UCM model [16] is chosen:

$$\boldsymbol{\tau} + \lambda \left[\frac{\partial \tau}{\partial t} + \nabla \cdot \boldsymbol{u}\boldsymbol{\tau} \right] = \lambda(\boldsymbol{\tau} \cdot \nabla \boldsymbol{u} + \nabla \boldsymbol{u}^{\mathrm{T}} \cdot \boldsymbol{\tau}) + \eta(\nabla \boldsymbol{u} + \nabla \boldsymbol{u}^{\mathrm{T}}). \tag{3}$$

This viscoelastic model exhibits both a constant shear viscosity η and first normal-stress coefficient (and hence relaxation time) allowing us to probe the effects of elasticity without the complications of shear thinning of either the shear viscosity or relaxation time.

A fully implicit finite-volume numerical method is used to solve Eqs. (1)–(3). The original numerical method, and subsequent developments, has been described in great detail in Oliveira et al. [17], Oliveira [18] and Alves et al. [19] and so is not unnecessarily repeated here. In the current study we essentially use the same methodology described in [19] except that here we use the QUICK scheme of Leonard [20] in preference to the CUBISTA scheme of Alves et al. [21] for the discretization of the convective terms in Eq. (3). The main disadvantage of the QUICK scheme, in comparison to its bounded versions (e.g. CUBISTA or SMART [22]) is its unbounded behaviour in highly convective flows, which can lead to strong oscillations and convergence problems when stepwise profiles are advected. Nevertheless, as a consequence of the smooth geometry used in this work, which contains no geometric singularities, the QUICK scheme is well behaved and can be used without convergence problems, thus avoiding the unnecessary numerical complications of the use of high-resolution schemes.

3. Geometry and computational meshes

Motivated by a desire to reach high Deborah numbers, and taking inspiration from a three-dimensional geometry used in the recent experimental study of Poole et al. [23] where large off-centre maxima were observed, we chose to use a 'smooth' contraction in preference to the abrupt geometries usually employed in contraction flow studies. A schematic of the geometry is shown in Fig. 1. Basically we have two planar channels, the larger (inlet) one having a half-height H_1 and the other (entrant) channel H_2 connected by two arcs (one convex, the other concave) of constant radius of curvature, $R = H_1 - H_2$. Defining the contraction ratio as CR ($=H_1/H_2$) we can also express this radius of curvature as $R = (\mathrm{CR} - 1)H_2$. The coordinate system is set around the symmetry plane at the "entrance" to the smaller channel. Although non-standard such geometries have many advantages over abrupt contractions especially for numerical studies such as this. The geometry is smooth and free of geometrical singularities and sharp corners where it is known that, even for a Newtonian fluid, the stresses and pressure become unbounded [24–26]. A constant wall radius of curvature

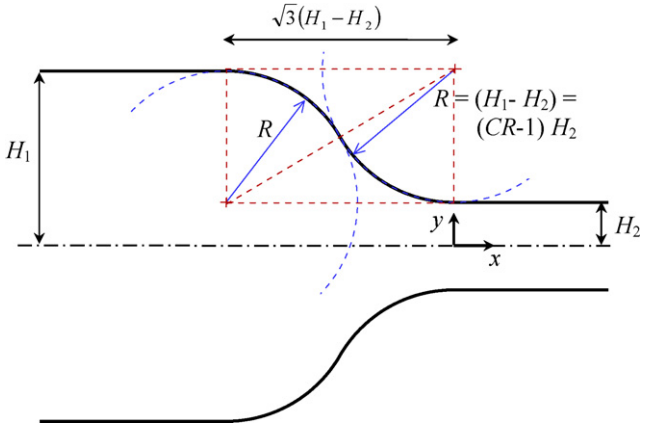

Fig. 1. Schematic of smooth contraction geometry.

is prescribed which, as we shall show, is extremely useful for predicting the onset of purely-elastic instabilities. In addition the geometry encourages the flow to remain attached to the walls and inhibits flow separation. Although the strain rate in such geometries is not constant, the absence of any recirculation makes an approximate estimation of the strain rate along the centreline possible.

As we are interested here in truly creeping flow (i.e. $Re = 0$) of a UCM fluid, the only non-dimensional parameters of relevance are those of the Deborah number which here we define based on downstream quantities, $De = \lambda U_2/H_2$, and the contraction ratio $\mathrm{CR} = H_1/H_2$. We note that in a real flow although the Reynolds number may be small, it will never be zero, as we assume in the present simulations in order to demonstrate that inertia is not necessary to induce divergent flow in contractions.

To study the effect of contraction ratio we investigated eight different geometries of varying contraction ratio (CR = 1.01, 1.1, 1.5, 2, 4, 8, 12 and 16). The meshes used are structured and non-orthogonal, and were created in such a way that the cells are approximately aligned with the streamlines in the Newtonian case. Although under steady conditions we expect the flow to remain symmetric about the centreline (i.e. $y = 0$), we decided to model the full domain in order to be able to capture any possible asymmetries that may develop due to the onset of a purely elastic instability.

For each contraction ratio a set of two different meshes was generated, which we denote by mesh M1-CR and M2-CR, where CR represents the contraction ratio under consideration. With mesh refinement (i.e. M1 to M2) the number of cells in each direction is doubled and the expansion/contraction factors are square-rooted in order to consistently halve the size of the cells in each direction. All the calculations presented here were carried out in the most refined meshes (i.e. M2-CR). The number of cells and the minimum cell sizes of the meshes varied depending on the contraction ratio. For meshes M2-CR the total number of cells varied from 40,352 (CR = 4) up to 63,360 (CR = 1.01). The streamwise minimum cell sizes varied from $\Delta x_{\min}/H_2 = 0.00020$ (CR = 1.01) up to $\Delta x_{\min}/H_2 = 0.028$ (CR = 8) while the minimum cell size in the transverse direction ranged from $\Delta y_{\min}/H_2 = 0.0003$ (CR = 1.01) up to $\Delta y_{\min}/H_2 = 0.01$ (CR $\geq$ 1.5). The differences observed in the results between meshes M1-CR and M2-CR are practically negligible: differences in the centreline velocities were below 2% for CR = 16 and CR = 2, for example.

4. Results and discussion

Firstly we focus our attention on the appearance or otherwise of the divergent regime, before in Section 4.2 discussing the mechanism for the occurrence of a purely elastic instability at high Deborah numbers.

4.1. Divergent flow regime

Streamline patterns for the 16:1, 4:1 and 2:1 contractions are shown in Fig. 2 for both the Newtonian case and a "high" Deborah number. As inspection of Fig. 2(a) readily shows, for the

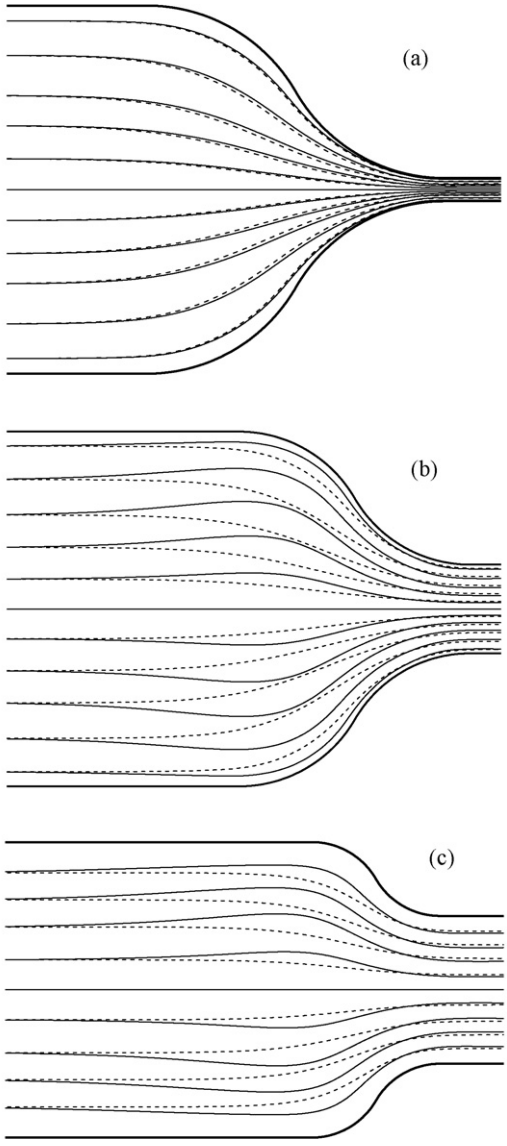

Fig. 2. Streamline patterns for (a) CR = 16: Newtonian (- - -) and $De = 25$ (—) superimposed; (b) CR = 4: Newtonian (- - -) and $De = 12$ (—) superimposed; (c) CR = 2: Newtonian (- - -) and $De = 6$ (—) superimposed.

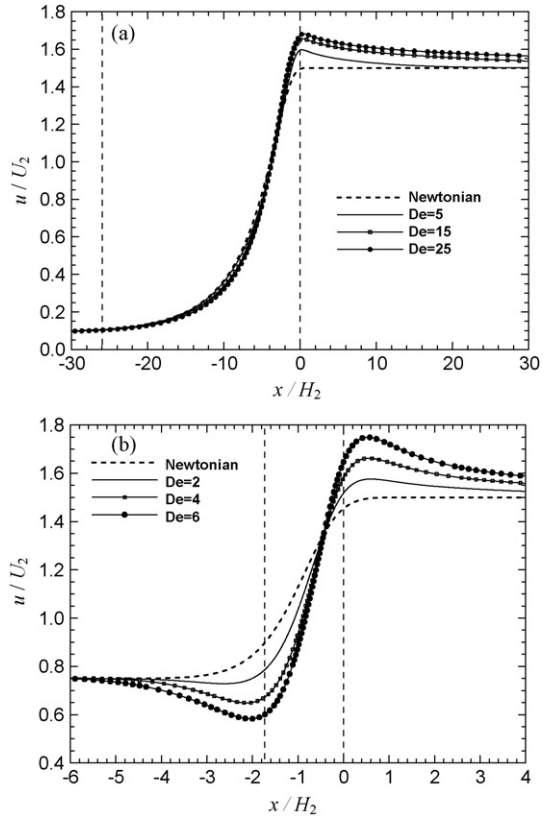

Fig. 3. Variation of streamwise velocity along centreline for (a) CR = 16 and (b) CR = 2. The vertical dashed lines indicate the beginning and the end of the contraction.

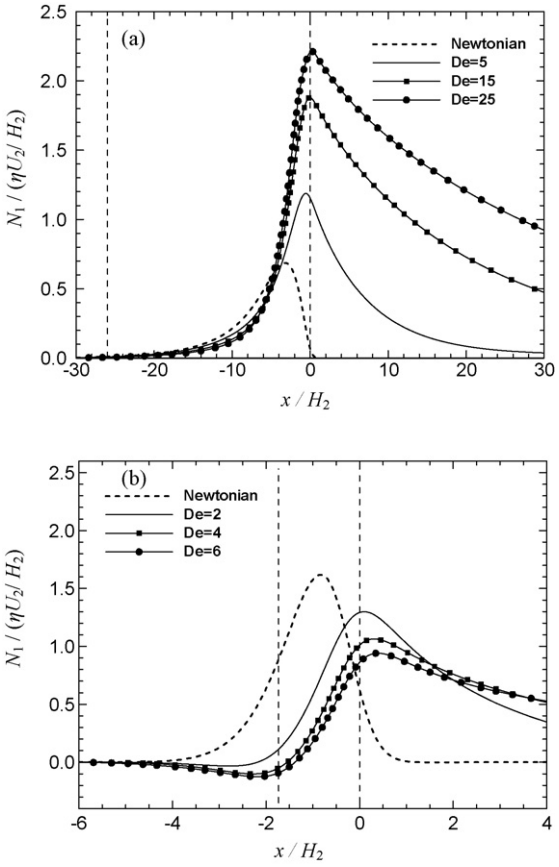

Fig. 4. Variation of first normal-stress difference along centreline for (a) CR = 16 and (b) CR = 2. The vertical dashed lines indicate the beginning and the end of the contraction.

higher contraction ratio, the effect of elasticity on the flow field is small and divergent flow is not observed. To highlight the small changes brought about by elasticity we show the Newtonian and $De = 25$ streamlines superimposed: the streamlines in the viscoelastic case are closer to the wall than the Newtonian but even this effect is small. Profiles of the streamwise velocity along the centreline, shown in Fig. 3(a), confirm that the velocity does not exhibit an undershoot characteristic of divergent flow. A small velocity overshoot, close to the inlet of the smaller channel, is in evidence in agreement with viscoelastic flows in abrupt contractions [27]. The variation of the first normal-stress difference (i.e. $N_1 = \tau_{xx} - \tau_{yy}$) along the centreline is shown in Fig. 4(a) and exhibits an increase with increasing De.

If we now turn our attention to a smaller contraction ratio (e.g. CR = 4) we observe divergent flow behaviour in the streamlines shown in Fig. 2(b) for the viscoelastic case. Reducing the contraction ratio still further, e.g. to CR = 2, makes the effect even more pronounced as shown in Fig. 2(c). For both contraction ratios the effect is again most readily observed by superposition of the corresponding Newtonian streamlines with the (approximately) highest Deborah number that steady solutions could be obtained in each geometry ($De = 12$ and 6, respectively). These results demonstrate that inertia is not a necessary condition for divergent flow to occur and, if one wishes to enhance such behaviour, it is preferable to investigate *small* contraction ratios. The corresponding variation of the centreline velocity for CR = 2 is shown in Fig. 3(b) and the characteristic velocity undershoot upstream of the contraction is now clearly visible. The variation of dimensionless first normal-stress difference along the centreline, plotted in Fig. 4(b), exhibits a *decrease* with increasing De, in marked contrast with the results presented in Fig. 4(a) for CR = 16.

To quantify the intensity of diverging flow, and to provide an indication as to the onset De, we find it useful to define an undershoot parameter, κ. This parameter represents the difference between the upstream fully-developed and the minimum centreline velocities, suitably non-dimensionalised by the minimum of either the difference between the fully-developed centreline velocities in the downstream ($U_{2,c}$) and upstream ($U_{1,c}$) channels or simply $U_{1,c}$:

$$\kappa = \frac{U_{1,c} - U_{\min}}{\min[U_{1,c}; U_{2,c} - U_{1,c}]} = \frac{U_{1,c} - U_{\min}}{U_{1,c}} \frac{1}{\min[1; (\mathrm{CR} - 1)]}. \quad (4)$$

Our rationale for this normalization (i.e. the denominator of Eq. (4)) was to highlight the degree of velocity undershoot in geometries of significantly different contraction ratio. The *obvious* velocity scale would be $U_{1,c}$, which limits the κ parameter between 0 (no undershoot) and 1 (zero velocity at centreline). However, for small contraction ratios this normalization would constrain the κ parameter to small values. A better alternative, for small CR, is to normalize the velocity undershoot with

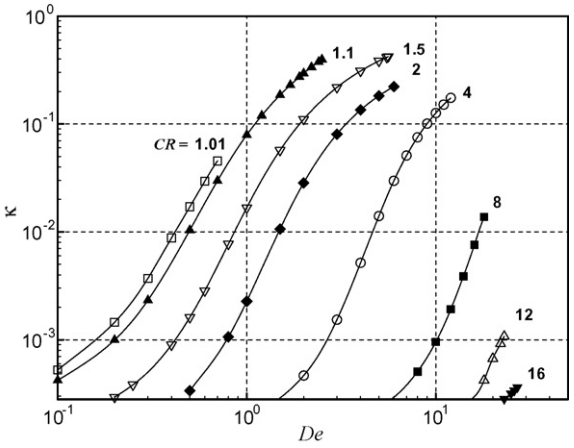

Fig. 5. Normalized velocity undershoot along centreline vs. Deborah number.

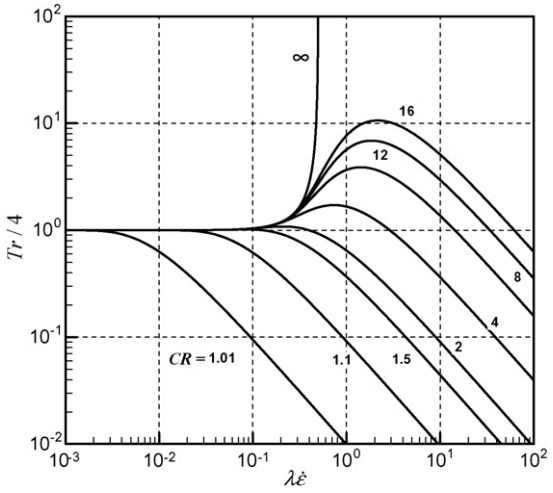

Fig. 6. Variation of Trouton ratio along the centreline within contraction with reduced strain rate for various contraction ratios.

$U_{2,c} - U_{1,c}$ since in this manner the κ parameter better reflects the intensity of diverging flow as compared with the curvature of the smooth contraction. Therefore, normalizing by the minimum of either of these two quantities is a reasonable compromise. Fig. 5 shows the variation of this undershoot parameter for the complete range of CRs. This quantitative measure of diverging flow is in general agreement with the more subjective visual indication of such behaviour seen in the streamline plots of Fig. 2.

In a flow of mixed shear and extensional nature, such as that considered here, it is likely that the onset of divergent flow may be a consequence of a change in the balance of the stresses within the flow from a flow that is shear dominated to one which is extensionally dominated. To attempt to quantify such a transition it is possible (c.f. [28] for example) to compare the normal stresses generated by the shear flow at the walls to the purely extensional normal stresses along the centreline through a dimensionless normal-stress ratio:

$$\aleph = \frac{N_1/\eta\dot{\gamma}}{(\tau_{xx} - \tau_{yy})/\eta\dot{\varepsilon}}. \tag{5}$$

For the UCM model in the shear-flow near the wall we can simply state that $N_1 = 2\lambda\eta\dot{\gamma}^2$. We can also estimate the maximum shear rate at the wall as being $\dot{\gamma} \approx 3U_2/H_2$. Along the centreline of the planar contraction, because the flow is purely extensional in nature it is possible to derive analytical expressions for the two non-zero normal stresses directly from the UCM constitutive equation (i.e. Eq. (3)). In such a flow Eq. (3) reduces to

$$\lambda u \frac{\partial \tau_{xx}}{\partial x} + \tau_{xx} = 2\eta\dot{\varepsilon} + 2\lambda\tau_{xx}\dot{\varepsilon} \tag{6a}$$

$$\lambda u \frac{\partial \tau_{yy}}{\partial x} + \tau_{yy} = -2\eta\dot{\varepsilon} - 2\lambda\tau_{yy}\dot{\varepsilon} \tag{6b}$$

where $\dot{\varepsilon} = \partial u/\partial x$ is the local strain rate. Assuming that the strain rate within the contraction is approximately constant (allowing us to express the velocity u at any location within the contraction as $u = U_1 + \dot{\varepsilon}(x + L)$, where L is the length over which the velocity increases linearly) and integrating we obtain (for $-L \le x \le 0$)

$$\tau_{xx} = 2\eta\frac{\dot{\varepsilon}}{1 - 2\lambda\dot{\varepsilon}}\left[1 - \left(1 + \frac{\dot{\varepsilon}(x + L)}{U_1}\right)^{-(1-2\lambda\dot{\varepsilon})/\lambda\dot{\varepsilon}}\right] \tag{7a}$$

$$\tau_{yy} = -2\eta\frac{\dot{\varepsilon}}{1 + 2\lambda\dot{\varepsilon}}\left[1 - \left(1 + \frac{\dot{\varepsilon}(x + L)}{U_1}\right)^{-(1+2\lambda\dot{\varepsilon})/\lambda\dot{\varepsilon}}\right]. \tag{7b}$$

At $x = 0$ (i.e. at the end of the contraction) the stresses attain their maximum (absolute) value and we can thus express the maximum Trouton ratio along the centreline as:

$$Tr \equiv \frac{\eta^E}{\eta} = \frac{\tau_{xx} - \tau_{yy}}{\eta\dot{\varepsilon}} = \frac{4}{(1 - 2\lambda\dot{\varepsilon})(1 + 2\lambda\dot{\varepsilon})} - \frac{2}{1 - 2\lambda\dot{\varepsilon}}\mathrm{CR}^{-(1-2\lambda\dot{\varepsilon})/\lambda\dot{\varepsilon}} - \frac{2}{1 + 2\lambda\dot{\varepsilon}}\mathrm{CR}^{-(1+2\lambda\dot{\varepsilon})/\lambda\dot{\varepsilon}}. \tag{8}$$

Substitution of Eq. (8), together with our estimates for N_1 and the shear rate at the wall, into Eq. (5) gives the following relationship for the normal-stress ratio:

$$\aleph = \frac{6De}{Tr} \tag{9}$$

where Tr is calculated from Eq. (8) and is illustrated in Fig. 6 as a function of $\lambda\dot{\varepsilon}$ and CR.

Finally to relate such behaviour to the 'divergent flow' phenomena we need to define a characteristic reduced strain rate (since Tr depends on CR and $\lambda\dot{\varepsilon}$):

$$\lambda\dot{\varepsilon} \approx \lambda\frac{U_{2,c} - U_{1,c}}{H_1} = \frac{3\lambda}{2}\frac{U_2 - U_1}{H_1} = \frac{3}{2}\frac{U_2\lambda}{H_2}\left(\frac{\mathrm{CR} - 1}{\mathrm{CR}^2}\right) = \frac{3}{2}\frac{De(\mathrm{CR} - 1)}{\mathrm{CR}^2}. \tag{10}$$

In this expression we are assuming that the approximate linear velocity profiles occur over a length $L = H_1$. In fact the contraction extends over a total length of $\sqrt{3}(H_1 - H_2)$ (see Fig. 1)

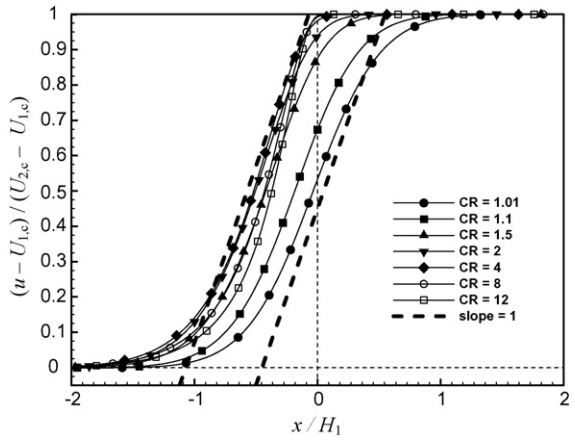

Fig. 7. Comparison of estimated strain rate (Eq. (10)) against centerline velocity profiles for various contraction ratios.

but, as can be observed in Fig. 7, especially for lower contraction ratios, the estimate $\dot{\varepsilon} \approx (U_{2,c} - U_{1,c})/H_1$ is indeed very good. For higher CR geometries this estimation deteriorates somewhat but is still, at worst, within about a factor of two of the exact value.

In Fig. 8(a) we plot the variation of the normal-stress ratio with *De* for each of the contraction ratios for which we have data together with an indication of the (approximate) *De* corresponding to the onset of divergent flow for each contraction ratio (estimated from Fig. 5 and assuming arbitrarily that the onset of diverging flow occurs when $\kappa \geq 10^{-3}$). It is clear that divergent flow does not occur at the same value of $\aleph$ for each contraction ratio. However, if we now plot the *gradient* of the normal-stress ratio, $\alpha \equiv \mathrm{d}[\log(\aleph)]/\mathrm{d}[\log(De)]$, against *De* (Fig. 8(b)) we can conclude that the onset of diverging flow occurs for each contraction ratio when α is approximately constant and slightly higher than one, indicating that diverging streamlines appear when the normal-stress ratio increases more rapidly than *De*.

The choice of $\kappa = 10^{-3}$ to quantify the onset of divergent flow is somewhat arbitrary, but using other κ values would lead to a similar conclusion. To demonstrate this, in Fig. 9 we illustrate the strong correlation between α and κ, showing unequivocally that the diverging flow intensity is directly related with the rate of increase of $\aleph$ with *De* (i.e. with α). For the UCM model the increase of α is due to a decrease of *Tr* with an increase in $\lambda\dot{\varepsilon}$ (or *De*, c.f. Eq. (9)). Thus, if instead of investigating the normal-stress ratio we simply turn our attention to the first normal-stress differences along the centreline (or to the Trouton ratio derived in Eq. (8)), the arguments given above become a little clearer. In Fig. 6 the maximum Trouton ratio is plotted against a general reduced strain rate and in Fig. 10 against the Deborah number based on our characteristic reduced strain rate (i.e. $De = 2\mathrm{CR}^2\lambda\dot{\varepsilon}/[3(\mathrm{CR}-1)]$). One of the well known "failures" of the UCM model is that the steady-state extensional viscosity becomes unbounded when $\lambda\dot{\varepsilon} \to 1/2$ [27]. However, in a contraction flow this limiting behaviour would only be observed if the contraction ratio was *infinite*. As can be seen in Figs. 6 and 10, for all finite contraction ratios, the Trouton ratio goes through

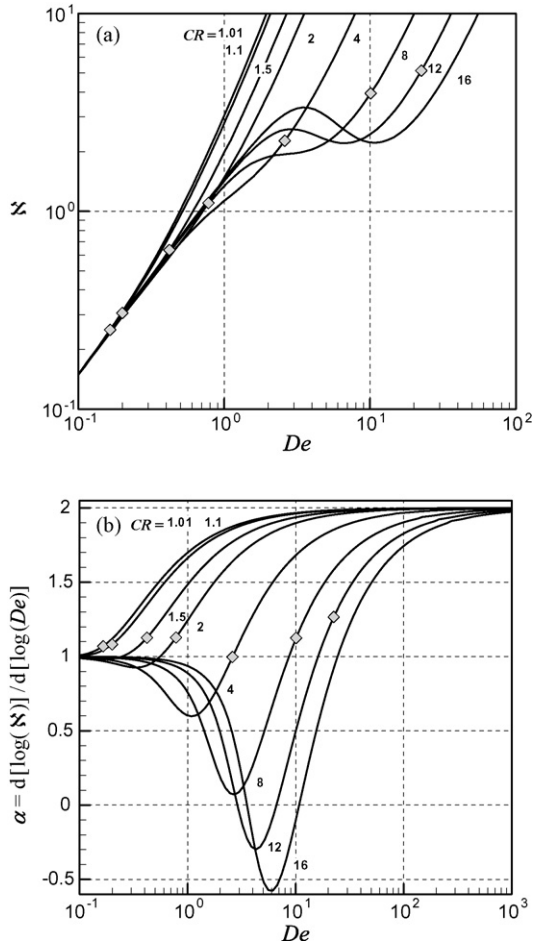

Fig. 8. (a) Normal-stress ratio vs. *De* for various contraction ratios. (b) Variation of gradient of normal-stress ratio vs. *De* for various contraction ratios. The symbols indicate the onset of divergent flow ($\kappa = 10^{-3}$).

a maximum and then decreases. Also included in Fig. 10 are symbols highlighting the Deborah numbers corresponding to the approximate onset of diverging flow behaviour (i.e. from Fig. 5). We hypothesize that it is the occurrence of such maxima in the Trouton ratio that leads to the onset of divergent flow (since α becomes higher than 1). If the fluid wishes to minimise the energy losses as it flows through the contraction then, when

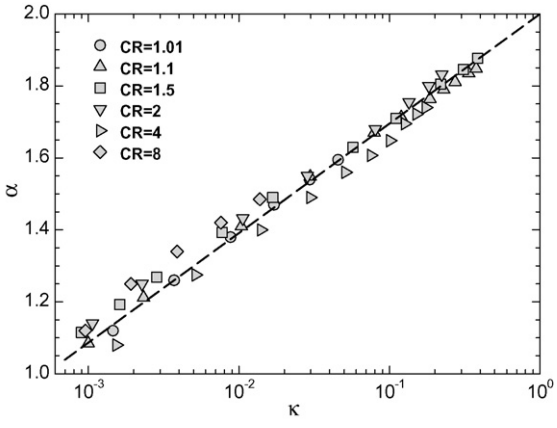

Fig. 9. Correlation between α and κ for various contraction ratios.

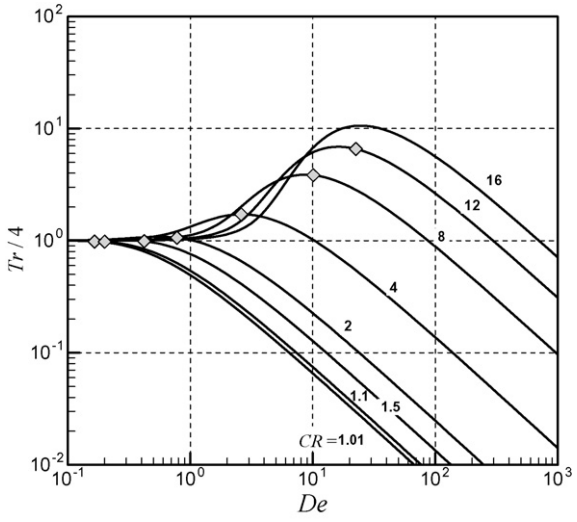

Fig. 10. Variation of Trouton ratio along the centreline within contraction with *De* for various contraction ratios. The symbols indicate the onset of divergent flow ($\kappa = 10^{-3}$).

it is in a regime close to the maxima value of *Tr*, it is actually beneficial for the strain rate along the centreline to *increase* as this will result in a decrease in *Tr*.

As a consequence of utilising a 'smooth' geometry to investigate the phenomena of diverging flow, an obvious question that arises about our results are their universality and, in particular, their relation to flow in abrupt contractions. As our explanation for the phenomena is essentially based on the maximum Trouton ratio (i.e. Eq. (8)) which, in fact, makes no assumption about the 'shape' of the contraction (just that the strain rate within the contraction is approximately constant) the conclusions drawn above are equally as valid for viscoelastic flow in abrupt (or sudden) contractions. To illustrate this statement we have performed additional simulations for inertialess flow of a UCM fluid in a 2:1 abrupt planar contraction. Again, divergent flow was observed for the higher Deborah values (for example, at $De = 2$ the normalized velocity undershoot in the centreline was $\kappa = 0.035$).

4.2. Onset and scaling of a purely elastic instability

As we have already briefly discussed, above a critical Deborah number steady numerical solutions could no longer be obtained and it was found that the flow became time-dependent. This critical Deborah number, De_{crit}, was observed to be strongly dependent on the value of the contraction ratio. Such purely elastic instabilities (i.e. in which inertia plays no role) have been observed experimentally in various different geometries: Taylor–Couette flow [29], contraction flow [30], lid-driven cavity flows [31] amongst many others. It is now well accepted that the destabilizing mechanism which leads to such instabilities is a combination of large normal stresses (which lead to tension along the fluid streamlines) and streamline curvature. McKinley et al. [1] proposed that the curvature of the flow and the tensile stress along the streamlines could be combined to form a dimensionless criterion that must be exceeded for the onset of purely elastic instabilities. They expressed this criterion for the onset of elastic instability in the general form:

$$\left[\frac{\lambda U}{\Re}\frac{\tau_{11}}{\eta\dot{\gamma}}\right]^{1/2} \geq M_{\text{crit}} \tag{11}$$

where λ is the relaxation time of the fluid, U the local streamwise fluid velocity, $\Re$ the local radius of curvature of the streamline, τ_{11} the local tensile stress in the flow direction, η the shear viscosity of the fluid and $\dot{\gamma}$ is the local shear rate. Far from the centreline the flow is shear dominated, thus it is legitimate to set

$$\tau_{11} = 2\lambda\eta\dot{\gamma}^2 \tag{12}$$

and substitution of this relationship into Eq. (11) gives

$$\left[\frac{\lambda U}{\Re}\lambda\dot{\gamma}\right]^{1/2} \geq \frac{M_{\text{crit}}}{\sqrt{2}}. \tag{13}$$

The first term on the left hand side of Eq. (13) can be thought of as a local Deborah number based on the streamline curvature (i.e. $\lambda U/\Re$) and the right hand term on the left hand side as a local Weissenberg number (i.e. $\lambda\dot{\gamma}$). To estimate these local values we need first to consider where the 'critical regions' in the flow will occur (i.e. where the instability will initiate). Guided by our numerical results and by a simple scaling argument (i.e. where the flow will have locally higher values of $\sqrt{DeWe}$) we propose that this critical region is near to the smaller channel inlet (i.e. $x \approx 0$). In this critical region we estimate that the characteristic radius of curvature of the streamlines is approximately

$$\Re(y) \approx \frac{R}{y/H_2} = \frac{(\text{CR}-1)H_2}{y/H_2}. \tag{14}$$

This expression correctly predicts the radius of curvature at the wall (i.e. $y = H_2$; $\Re = (\text{CR}-1)H_2$) and along the centreline where the curvature of the streamline must be zero due to symmetry ($y = 0$; $\Re \to \infty$). Comparison of this simple form of the characteristic radius with streamlines actually predicted from our numerical results close to the critical *De*, not shown here for conciseness, shows excellent agreement in the 'critical' region close to the inlet of the smaller channel. If we also make the (approximate) assumption that the velocity profile near $x = 0$ is parabolic (i.e. corresponds to instantaneously fully-developed channel flow), then at the critical axial position ($x = 0$)

$$U(y) \approx \frac{3}{2}U_2\left[1 - \left(\frac{y}{H_2}\right)^2\right]. \tag{15}$$

The local deformation rate in this critical region is

$$\dot{\gamma}(y) \approx 3\frac{U_2}{H_2}\frac{y}{H_2} \tag{16}$$

and substitution of Eqs. (14)–(16) into the stability criterion (i.e. Eq. (13)) leads to:

$$\left[\frac{1}{\text{CR}-1}\left(\frac{\lambda U_2}{H_2}\right)^2\left[1 - \left(\frac{y}{H_2}\right)^2\right]\left(\frac{y}{H_2}\right)^2\right]^{1/2} \geq \frac{M_{\text{crit}}}{3}. \tag{17}$$

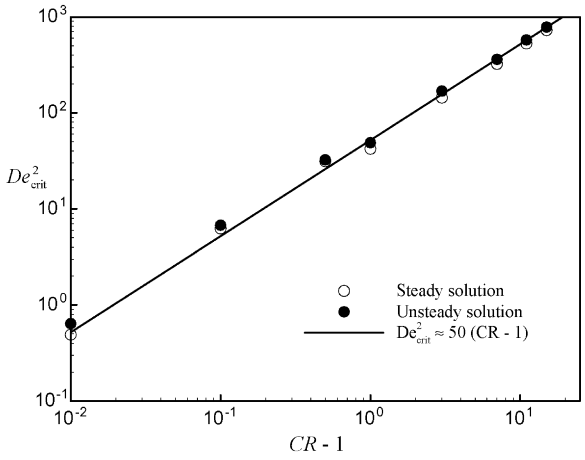

Fig. 11. Variation of critical *De* for onset of elastic instability vs. contraction ratio.

We can now easily estimate that the transverse location where the instability sets in is $y/H_2 = 1/\sqrt{2}$ by simply finding the y position where the left hand side of Eq. (17) is a maximum. Thus, at the critical location ($x = 0$; $y = H_2/\sqrt{2}$) we arrive at the following equation for the onset of purely elastic instabilities in our geometry:

$$\left[\frac{1}{\mathrm{CR}-1}\left(\frac{\lambda U_2}{H_2}\right)^2_{\mathrm{crit}}\right] \geq \frac{2}{3}M_{\mathrm{crit}}. \tag{18}$$

Realising that we have defined our (global) Deborah number as $De = \lambda U_2/H_2$ and rearranging we arrive finally at

$$De^2_{\mathrm{crit}} = \tfrac{4}{9}M^2_{\mathrm{crit}}(\mathrm{CR}-1). \tag{19}$$

The values of De^2_{crit} determined numerically are plotted together with a linear fit versus CR − 1 in Fig. 11 showing excellent agreement with this linear scaling. Although such a linear scaling with contraction ratio may, at first, seem surprising as it implies that as the contraction ratio tends to one (i.e. to a planar channel) the critical Deborah number tends to zero, it is purely a consequence of our geometry where, as the contraction ratio decreases, the local curvature of the streamlines becomes increasingly sharp. In addition it is perhaps unlikely that our definition of the characteristic radius of curvature for the streamlines will remain applicable close to the limit of CR → 1. Nevertheless, our numerical results shown in Fig. 11 are in general agreement with the linear scaling even at low contraction ratios where the critical *De* is seen to be less than 1 for a contraction ratio of 1.01 (i.e. only a 1% perturbation from a planar channel).

5. Conclusions

This work reports the results of a systematic numerical investigation, using the UCM model, of creeping flow through "smooth" planar contractions. It was shown that strongly divergent flow can occur in such cases in contrast to the existing results in the literature where the phenomena is usually attributed to the interplay between inertial and elastic stresses. It was demonstrated that such behaviour is more likely to be observed in small contraction ratios and using a straightforward theoretical analysis we have shown that it can be approximately predicted from the material functions of the fluid.

Above a critical Deborah number, which was found to vary with contraction ratio, a purely elastic instability sets in, and the flow becomes time-dependent. Using a simple analysis, based on the scaling arguments of McKinley et al. [1], it was shown that De^2_{crit} varies linearly with contraction ratio in excellent agreement with the numerical results.

The use of "smooth" contraction geometries, although non-standard, proved to offer many advantages over the typical abrupt contractions and, aside from the absence of vortex enhancement, seems to offer an excellent complimentary geometry in which to study viscoelastic effects in contraction flows.

Acknowledgements

The authors would like to thank the British Council/Conselho de Reitores das Universidades Portuguesas for support through the 'Treaty of Windsor Programme' (LIS/992 (2005/06) U17 & Acção n° B-17/05). MAA acknowledges funding by Fundação para a Ciência e a Tecnologia (FCT, Portugal) and FEDER under project POCI/EQU/59256/2004. RJP also acknowledges funding from the Royal Society. The stimulus for this study arose from a fruitful conversation with Professor Gareth McKinley: this and subsequent valuable discussions are gratefully acknowledged.

References

[1] G.H. McKinley, P. Pakdel, A. Oztekin, Rheological and geometric scaling of purely elastic flow instabilities, J. Non-Newtonian Fluid Mech. 67 (1996) 19–47.
[2] P.J. Cable, D.V. Boger, Comprehensive experimental investigation of tubular entry flow of viscoelastic fluids. 3. Unstable flow, AIChE J. 25 (1) (1979) 152–159.
[3] P.J. Cable, D.V. Boger, Comprehensive experimental investigation of tubular entry flow of viscoelastic fluids. 2. Velocity-field in stable flow, AIChE J. 24 (6) (1978) 992–999.
[4] P.J. Cable, D.V. Boger, Comprehensive experimental investigation of tubular entry flow of viscoelastic fluids. 1. Vortex characteristics in stable flow, AIChE J. 24 (5) (1978) 869–879.
[5] D.V. Boger, K. Walters, Rheological Phenomena in Focus, Elsevier, New York, 1993.
[6] P.J. Cable, Laminar Entry Flow of Viscoleastic Liquids, PhD Thesis, Monash University, 1976.
[7] D.V. Boger, Highly elastic constant-viscosity fluid, J. Non-Newtonian Fluid Mech. 3 (1) (1977) 87–91.
[8] D.V. Boger, R.J. Binnington, Circular entry flows of fluid M1, J. Non-Newtonian Fluid Mech. 35 (2/3) (1990) 339–360.
[9] R.E. Evans, K. Walters, Further remarks on the lip-vortex mechanism of vortex enhancement in planar-contraction flows, J. Non-Newtonian Fluid Mech. 32 (1) (1989) 95–105.
[10] R.E. Evans, K. Walters, Flow characteristics associated with abrupt changes in geometry in the case of highly elastic liquids, J. Non-Newtonian Fluid Mech. 20 (1986) 11–29.
[11] L.E. Rodd, T.P. Scott, D.V. Boger, J.J. Cooper-White, G.H. McKinley, The inertio-elastic planar entry flow of low-viscosity elastic fluids in micro-fabricated geometries, J. Non-Newtonian Fluid Mech. 129 (1) (2005) 1–22.

[12] M.A. Hulsen, Numerical simulation of the divergent flow regime in a circular contraction flow of a viscoelastic fluid, Theor. Comput. Fluid Dyn. V5 (1) (1993) 33–48.
[13] N. Phan-Thien, R.I. Tanner, A new constitutive equation derived from network theory, J. Non-Newtonian Fluid Mech. 2 (4) (1977) 353–365.
[14] B. Purnode, M.J. Crochet, Flows of polymer solutions through contractions. 1. Flows of polyacrylamide solutions through planar contractions, J. Non-Newtonian Fluid Mech. 65 (2/3) (1996) 269–289.
[15] R.B. Bird, R.C. Armstrong, O. Hassager, Dynamics of polymeric liquids Fluid Mechanics, vol. 1, Wiley, New York, 1987.
[16] J.G. Oldroyd, On the formulation of rheological equations of state, Proc. R. Soc. London Seri. Math. Phys. Sci. 200 (1063) (1950) 523–541.
[17] P.J. Oliveira, F.T. Pinho, G.A. Pinto, Numerical simulation of non-linear elastic flows with a general collocated finite-volume method, J. Non-Newtonian Fluid Mech. 79 (1) (1998) 1–43.
[18] P.J. Oliveira, On the numerical implementation of nonlinear viscoelastic models in a finite-volume method, Numer. Heat Transfer Part B-Fundam. 40 (4) (2001) 283–301.
[19] M.A. Alves, P.J. Oliveira, F.T. Pinho, Benchmark solutions for the flow of Oldroyd-B and PTT fluids in planar contractions, J. Non-Newtonian Fluid Mech. 110 (1) (2003) 45–75.
[20] B.P. Leonard, Stable and accurate convective modeling procedure based on quadratic upstream interpolation, Comput. Methods Appl. Mech. Eng. 19 (1) (1979) 59–98.
[21] M.A. Alves, P.J. Oliveira, F.T. Pinho, A convergent and universally bounded interpolation scheme for the treatment of advection, Int. J. Numer. Methods Fluids 41 (1) (2003) 47–75.
[22] P.H. Gaskell, A.K.C. Lau, Curvature-compensated convective-transport - smart, a new boundedness-preserving transport algorithm, Int. J. Numer. Methods Fluids 8 (6) (1988) 617–641.
[23] R.J. Poole, M.P. Escudier, P.J. Oliveira, Laminar flow of a viscoelastic shear-thinning liquid through a plane sudden expansion preceded by a gradual contraction, Proc. R. Soc. London Series A 461 (2064) (2005) 3827–3845.
[24] W.R. Dean, P.E. Montagnon, On the steady motion of viscous liquid in a corner, Proc. Camb. Philos. Soc. 45 (3) (1949) 389–394.
[25] H.K. Moffatt, Viscous and resistive eddies near a sharp corner, J. Fluid Mech. 18 (1) (1964) 1–18.
[26] E.J. Hinch, The flow of an oldroyd fluid around a sharp corner, J. Non-Newtonian Fluid Mech. 50 (2–3) (1993) 161–171.
[27] R.G. Owens, T.N. Phillips, Computational Rheology, Imperial College Press, London, 2002.
[28] J.P. Rothstein, G.H. McKinley, The axisymmetric contraction-expansion: the role of extensional rheology on vortex growth dynamics and the enhanced pressure drop, J. Non-Newtonian Fluid Mech. 98 (1) (2001) 33–63.
[29] R.G. Larson, E.S.G. Shaqfeh, S.J. Muller, A purely elastic instability in Taylor–Couette flow, J. Fluid Mech. 218 (1990) 573–600.
[30] G.H. McKinley, W.P. Raiford, R.A. Brown, R.C. Armstrong, Nonlinear dynamics of viscoelastic flow in axisymmetrical abrupt contractions, J. Fluid Mech. 223 (1991) 411–456.
[31] P. Pakdel, G.H. McKinley, Elastic instability and curved streamlines, Phys. Rev. Lett. 77 (12) (1996) 2459–2462.